Biomedicine & Pharmacotherapy 144 (2021) 112362

Contents lists available at ScienceDirect

Biomedicine & Pharmacotherapy

journal homepage: www.elsevier.com/locate/biopha

Designing new antitubercular isoniazid derivatives with improved reactivity and membrane trafficking abilities

Catarina Frazão de Faria [a,c], Tânia Moreira [a,c], Pedro Lopes [b], Henrique Costa [a,c], Jessica R. Krewall [d], Callie M. Barton [d], Susana Santos [a,c], Douglas Goodwin [d], Diana Machado [e], Miguel Viveiros [e], Miguel Machuqueiro [b,c,*], Filomena Martins [a,c,*]

[a] Centro de Química Estrutural, Faculdade de Ciências, Universidade de Lisboa, Campo Grande, C8 bdg, Lisboa 1749-016, Portugal
[b] BioISI – Biosystems & Integrative Sciences Institute, Faculty of Sciences, University of Lisboa, Campo Grande, C8 bdg, Lisboa 1749-016, Portugal
[c] Departamento de Química e Bioquímica, Faculdade de Ciências, Universidade de Lisboa, Lisboa 1749-016, Portugal
[d] Department of Chemistry and Biochemistry, Auburn University, Auburn 36849-5312, AL, USA
[e] Unidade de Microbiologia Médica, Global Health and Tropical Medicine, Instituto de Higiene e Medicina Tropical, Universidade Nova de Lisboa, Rua da Junqueira, 100, Lisboa 1349-008, Portugal

ARTICLE INFO

Keywords:
KatG
Molecular dynamics
Permeability
Activation
Synthesis
MIC
2000 MSC:
0000
1111
PACS:
0000
1111

ABSTRACT

Isoniazid (INH) is one of the two most effective first-line antitubercular drugs and is still used at the present time as a scaffold for developing new compounds to fight TB. In a previous study, we have observed that an INH derivative, an hydrazide *N'*-substituted with a C_{10}acyl chain, was able to counterbalance its smaller reactivity with a higher membrane permeability. This resulted in an improved performance against the most prevalent *Mycobacterium tuberculosis* (*Mtb*) resistant strain (S315T), compared to INH. In this work, we have designed two new series of INH derivatives (alkyl hydrazides and hydrazones) with promising *in silico* properties, namely membrane permeabilities and spontaneous IN* radical formation. The kinetics, cytotoxicity, and biological activity evaluations confirmed the *in silico* predictions regarding the very high reactivity of the alkyl hydrazides. The hydrazones, on the other hand, showed very similar behavior compared to INH, particularly in biological tests that take longer to complete, indicating that these compounds are being hydrolyzed back to INH. Despite their improved membrane permeabilities, the reactivities of these two series are too high, impairing their overall performance. Nevertheless, the systematic data gathered about these compounds have showed us the need to find a balance between lipophilicity and reactivity, which is paramount to devise better INH-based derivatives aimed at circumventing *Mtb* resistance.

1. Introduction

Tuberculosis (TB) is still one of the most deadly infectious diseases and about 25% of the global population is infected with *Mycobacterium tuberculosis* (*Mtb*), the causative agent of TB. Yet, TB is a largely preventable and treatable disease. The last World Health Organization (WHO) report on TB [1] estimated in 2019 the occurrence of 10 million new cases worldwide and about 1.4 million deaths. Additionally, about half a million people developed rifampicin (RIF)-resistant TB, of which 78% corresponded to multidrug-resistant tuberculosis, a form of TB that does not respond to at least the two most powerful first-line antitubercular drugs, RIF and isoniazid (INH). To make the scenario worse, a very recent media brief from STOP TB Partnership [2] recognized the dramatic impact of COVID-19 pandemic on TB, particularly in low- and middle-income countries, due to an enormous decline in TB diagnosis and treatment (a 23% decrease for nine of the high-TB burden countries). This is aggravated by an increased risk of adverse outcomes and mortality (3 times higher in people co-infected with SARS-CoV-2) [2].

Isoniazid (INH) is active solely against mycobacteria, in particular *Mtb*, with minimum inhibitory concentrations ranging from 0.02 to 0.1 μg/mL, and it penetrates the mycobacterial cell through passive diffusion [3]. INH is a prodrug that needs to be converted to its active form by the multifunctional catalase-peroxidase enzyme KatG. Once activated, INH forms an isonicotinoyl radical that binds to nicotinamide adenine dinucleotide (NAD^+), ultimately forming the IN-NAD adduct. IN-NAD binds and inactivates InhA, an NADH-dependent enoyl-acyl carrier

* Corresponding author at: Departamento de Química e Bioquímica, Faculdade de Ciências, Universidade de Lisboa, Lisboa 1749-016, Portugal.
E-mail addresses: machuque@ciencias.ulisboa.pt (M. Machuqueiro), feleitao@fc.ul.pt (F. Martins).

https://doi.org/10.1016/j.biopha.2021.112362
Received 16 September 2021; Received in revised form 14 October 2021; Accepted 19 October 2021
Available online 26 October 2021

protein reductase essential for mycolic acid biosynthesis [4]. As mycolic acids are essential constituents of the *Mtb* cell wall, this is the ultimate target of INH [5]. KatG-dependent activation of INH and subsequent inactivation of InhA results in an accumulation of long chains of fatty acids, inhibition of biosynthesis of mycolic acids, and loss of acid fastness. Consequently, the cell's surface wrinkles and bulges resulting in a deformed and swollen rod that ultimately bursts [3,5]. Isoniazid resistance is associated with a multiplicity of mutations affecting one or more genes, mainly, the genes *katG* and *inhA*. In clinical isolates of *Mtb*, the great majority of the mutations responsible for INH resistance occur in the *katG* gene, where the presence of repeated sequences makes it prone to high-level resistance mutations. The most common one is at codon 315, where a serine is substituted by a threonine (i.e., S315T KatG). Mutations in other genes also decrease affinity towards INH, especially the mutations in the *inhA* gene, resulting in the incapacity of INH (and ethionamide) to inhibit the mycolic acid synthesis, conferring low-level resistance (except when a combination of mutations in *katG* and in the *inhA* promoter region occur) [3]. Being one of the two most effective drugs of the standard anti-TB treatment regimen, resistance to INH, at any level, poses serious difficulties in the management of TB. Overcoming resistance towards INH is, therefore, a major challenge for drug discovery and new therapeutic regimens for TB include either the improvement of the therapeutic efficacy of INH or the search for synergistic effects in combination with other drugs [6].

In our previous work, we have devised a two-step computational protocol to generically estimate the stability and membrane permeability of INH derivatives [7]. In the first step, we used Quantum Mechanics (QM) calculations to estimate the reactivity of INH derivatives to spontaneously form the IN$^{\bullet}$radical. Membrane permeabilities were calculated using Molecular Dynamics (MD) simulations coupled with the umbrella sampling/potential of mean force protocols. Interestingly, KatG kinetics and minimum inhibitory concentration (MIC) values obtained for INH and their acylated derivatives could only be interpreted using a trade-off between the compounds' reactivity and membrane trafficking ability. Indeed, we observed that the acyl hydrazide INH-C_{10} counterbalances a significantly smaller reactivity by having a higher membrane permeability.

Based on our previous results, in this study, we aimed to design a new series of compounds that combine a high membrane permeability with reactivity to spontaneously form the IN$^{\bullet}$ radical that is similar to or better than INH. These new compounds were designed and initially tested *in silico* before their synthesis and subsequent assessment by *in vitro* KatG kinetics, as well as cytotoxicity and biological evaluation.

2. Methods

2.1. Quantum mechanics calculations

Quantum mechanical (QM) calculations were used to estimate the Gibbs free energies of formation, ΔG, following a previously described approach [7]. The reactions for the spontaneous activation of INH and its derivatives (Fig. 1) can be arranged in thermodynamic cycles to simplify the number of calculations needed:

$\Delta G^{INH} = G(IN^*) + G(H^+) + G(e^-) + G(N_2H_2) - G(INH)$.

$\Delta G^{INH-X} = G(IN^*) + G(H^+) + G(e^-) + G(N_2X) - G(INH\text{-}X)$.

$\Delta\Delta G = \Delta G^{INH-X} - \Delta G^{INH} = G(N_2X) - G(INH\text{-}X) - G(N_2H_2) + G(INH)$.

Following the proposed scheme, calculation of the Gibbs free energy of formation requires estimation of the free energies of H_2N_2, N_2X, INH, and INH-X. The mechanism assumes that a homolytic cleavage of the —(C═O)—NHN— bond occurs to form an isonicotinoyl radical (IN*), H_2N_2/N_2X, a proton, and an electron. This mechanism is slightly different in the case of the imine compound series (INH-iC_n). It is assumed that deprotonation still occurs, leading to the formation of IN* and the N^-═N^+═CH—R compounds, which were used in the calculations. All QM calculations were performed at the density functional theory (DFT) level with the M06 functional [8] and the aug-ccpVDZ

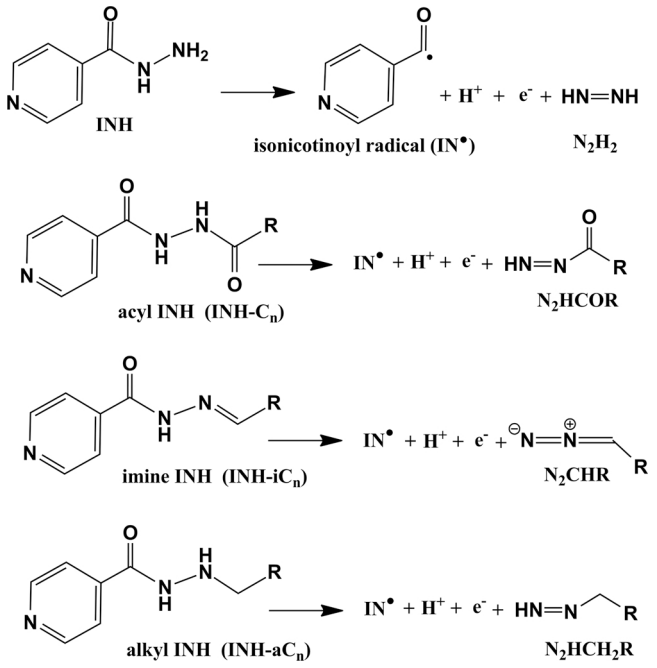

Fig. 1. Reactional scheme with products obtained from spontaneous activation of INH and its acyl, imine and alkyl derivatives. The R group stands for an aliphatic tail and *n* in the C_n suffix stands for the number of carbon atoms in the substituents. For a complete list of compounds used in this work, please see Table 1.

Dunning basis sets [9,10] The SMD implicit solvent model was used with the QM calculations [11]. These settings were also used in the QM geometry optimizations to prepare the different compounds for force field parameterization.

2.2. Molecular dynamics simulations

MD simulations coupled to steered MD and Umbrella Sampling protocols were performed to calculate *in silico* the membrane permeabilities of the INH derivatives. The protocol was similar for all systems. The membrane was modeled by a pre-equilibrated slab of 128 1-palmitoyl-2-oleoyl-*sn*-glycero-3-phosphocholine (POPC) lipids with 5941 water molecules [7,12,13]. The simulations were performed using GROMACS 2018.6 [14] and the GROMOS 54A7 force field [15,16]. Water molecules were described with the SPC water model [17]. The topologies were determined using the Automated Topology Builder (ATB) and Repository [18] and manually curated [19–21]. In particular, the ATB topologies were modified in the pairs section to exclude 1–4 interactions in the pyridyl fragment, following the GROMOS rules for aromatic rings. In the series of compounds with varying lengths of the aliphatic chain, the topologies were built for the shortest chain compound and propagated with additional methylene groups to fulfill the desired length. This approach favors parameter transferability and allows a more unbiased comparison between analogous compounds.

All simulations were performed within the NPT ensemble with the pressure (1 bar with a coupling constant of 2 ps) and temperature (298.15 K with a coupling constant of 0.1 ps) being kept constant using the Parrinello–Rahman barostat [22,23] and v-rescale thermostat [24], respectively. Semi-isotropic pressure coupling was used with the compressibility of 4.5×10^{-5} bar^{-1}. The particle mesh Ewald method was used for the electrostatic interactions with a real-space cutoff of 1.0 nm and a Fourier grid spacing of 0.12 nm. van der Waals interactions were truncated above 1.0 nm. All bonds were constrained using the P-LINCS algorithm [25] for membrane and solutes, and SETTLE [26] for water. The equations of motion were integrated every

2 fs with the neighbor lists being updated every 10 steps.

All starting systems were energy minimized to remove unfavorable interactions. In the minimization step, both the steepest descent and low-memory Broyden–Fletcher–Goldfarb–Shanno algorithms were used. The initialization was performed in two steps of 100 ps each: the first was performed at constant volume and the second with a temperature coupling constant of 0.01 ps to avoid large fluctuations. The different compounds were pulled across the lipid bilayer (at 10 nm ns^{-1} with a force constant of 1000 kJ mol^{-1} nm^{-2}) in a steered MD protocol to generate starting conformations for the US protocol. In this scheme, equally spaced umbrella windows (in intervals of 0.1 nm) ranging from the center of the bilayer (0 nm) to a distance of 3.5 nm (zero energy setting) were selected, corresponding to bulk water. Each umbrella was run for 150 ns (shorter chains) or 250 ns (longer chains) and the initial 20 ns were discarded in the potential of mean force (PMF) calculation to ensure convergence. The compounds were restrained using a bias force constant of 1000 kJ mol^{-1} nm^{-2} centered in the N' atom. The weighted histogram analysis method (WHAM) [27] was used for the PMF calculations. The permeability rates were calculated using the inhomogeneous solubility-diffusion model (ISDM) [28,29] coupled to the biasing harmonic potential [30,31]. The error values (standard error of the mean) were calculated from two segments obtained by splitting the converged data into two halves, which were treated as independent.

3. Results and discussion

3.1. Proposal of new INH-derivatives with improved reactivities and membrane permeabilities

We have previously devised a strategy based on a thermodynamic cycle to estimate the Gibbs free energies of formation of the IN* radical starting from different prodrug compounds [7]. With this approach, we observed that two acylated INH derivatives (INH-C_2 and INH-C_{10}) were significantly deactivated, which could explain their lower experimental activities against wt-KatG. However, low MIC values were obtained for INH-C_{10}, especially in S315T mutated strains, which we attributed to an improved diffusion across cell membranes as compared with INH [7]. In this work, we have systematically calculated the reactivity of these INH acylated derivatives which included those not covered in our previous work (C_4 – C_8) (Fig. 2). Overall, the free energies of formation are very similar for the complete acylated series (Table 1), confirming that all compounds are very stable. In our previous work, due to a small error in our procedure, the membrane permeabilities reported for INH, INH-C_2, and INH-C_{10} [7] were erroneously multiplied by a factor of 2. Even though this did not affect the relative quantitative interpretation of the data, we decided to include those compounds also in this study, which follows a protocol that benefits from longer simulations, hence better sampling. The membrane permeabilities of the acylated series showed a gradual increase with the size of the aliphatic chain (Table 1). Excluding INH-C_2, all other acylated compounds have improved membrane permeabilities as compared with INH, which indicates that the improved MIC values observed for INH-C_{10}, compared to INH-C_2 [32], could have also been obtained, at least partially, for other shorter chain compounds like INH-C_8 or INH-C_6.

Table 1
Isonicotinoyl radical Gibbs free energies of formation, and membrane permeabilities for INH and all its derivatives used in this work (see their chemical structures in Fig. 2). The $\Delta\Delta G$ values for INH, INH-C_2, and INH-C_{10} were obtained from our previous work [7]. Even though we cannot estimate error values for the $\Delta\Delta G$ presented here, as a rule of thumb, we can assume at least 2 kcal/mol for most computational protocols. Please note that the membrane permeabilities of INH, INH-C_2, and INH-C_{10} were calculated incorrectly in our previous work (values were wrongly multiplied by 2) [7], and therefore they were recalculated using our protocol with improved sampling.

Compound	Number	$\Delta\Delta G$ (kcal/mol)	Permeability (cm s^{-1}) ± s.e.
INH	–	0.0	0.3 ± 0.1
INH-C_2	**1a**	9.1	0.5 ± 0.3
INH-C_4	**1b**	9.7	1.8 ± 0.1
INH-C_6	**1c**	8.9	2.2 ± 0.5
INH-C_8	**1d**	10.3	10.2 ± 2.1
INH-C_{10}	**1e**	10.8	12.1 ± 2.7
INH-iC_2	**2a**	-1.3	1.8 ± 0.1
INH-iC_4	**2b**	-1.3	2.5 ± 1.5
INH-iC_6	**2c**	-1.7	9.4 ± 1.5
INH-iC_8	**2d**	-2.8	10.5 ± 5.2
INH-iC_{10}	**2e**	-2.4	24.3 ± 5.5
INH-aC_2	**3a**	-6.8	0.5 ± 0.4
INH-aC_4	**3b**	-9.1	3.3 ± 0.7
INH-aC_6	**3c**	-9.8	5.5 ± 0.7
INH-aC_8	**3d**	-10.4	16.5 ± 0.7
INH-aC_{10}	**3e**	-10.5	29.2 ± 9.3

The results obtained with the acyl hydrazide series provided the starting point for the design of two new series of INH derivatives (Fig. 2), aiming at having similar or better reactivity profiles than INH while retaining improved membrane permeabilities like INH-C_{10}. The rationale was to modify the acyl moiety, which, being electron-withdrawing, weakens the N—N bond and, consequently, strengthens the adjacent amide bond, precisely the one that needs to be cleaved for IN* formation. With this in mind, and based on the acyl hydrazide scaffold, two homologous series of INH derivatives were designed: the hydrazone series (INH-iC_n), where the N' atom, instead of participating in an amide function, becomes part of a hydrazone moiety, and the N'-alkyl hydrazide (INH-aC_n) series, where the N' carbonyl group is deoxygenated (see

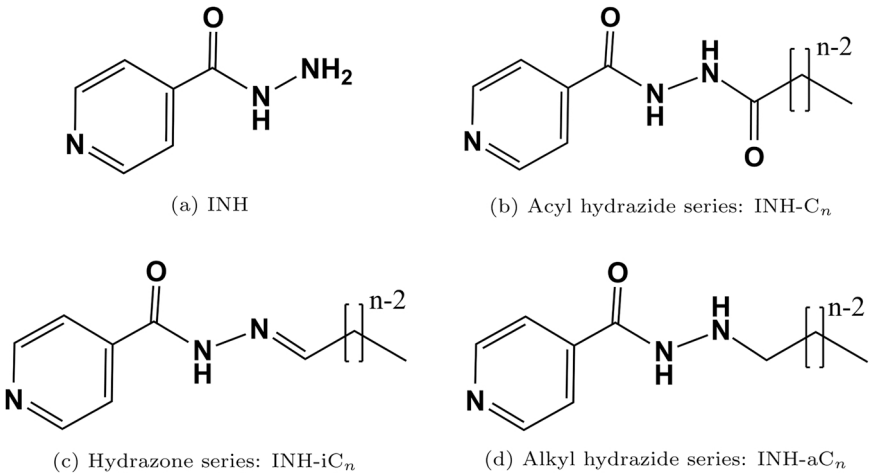

(a) INH (b) Acyl hydrazide series: INH-C_n

(c) Hydrazone series: INH-iC_n (d) Alkyl hydrazide series: INH-aC_n

Fig. 2. Chemical structure of INH and each of its three derivative series studied in this work.

Fig. 2). The reactivities for the spontaneous formation of the IN* radical were calculated, using a probably unstable zwitterionic final compound as a reference. The hydrazone series showed reactivities similar to INH (Table 1) which, complemented with improved membrane permeabilities (at least for the longer chains), can still lead to promising candidate compounds. The substitution of the *N′*-acyl group by an imino group produces an increase in the membrane permeabilities for a number of these new compounds. This higher permeability can be explained by a small reduction in the compounds' polarity and a likely destabilizing effect on their first water solvation shell, which should decrease the desolvation penalties upon membrane insertion. On the other hand, the compounds belonging to the alkyl hydrazide series, INH-aC_n showed free energies of formation ranging from −6.8 to −10.5 kcal/mol, for INH-aC_2 to INH-aC_{10}, respectively (Table 1). These $\Delta\Delta G$ values indicate that all these compounds should be very reactive, which was one of our objectives. They also show enhanced membrane permeabilities, which is particularly noticeable for the longer carbon chain compounds.

In summary, we estimated *in silico* the spontaneous reactivities towards isonicotinoyl radical formation of several INH derivatives, which allowed us to classify the compounds of the three designed series as deactivated (acyl hydrazide series, INH-C_n), INH-like activated (hydrazone series, INH-iC_n), and extremely activated (alkyl hydrazide series, INH-aC_n) molecules. The key factor influencing the reactivity seems to be the nature of the N′–C bond, whereas membrane permeability coefficients are mainly ruled by the length of the aliphatic carbon chain, resulting in similar permeability profiles independently of the *N′* substitution.

3.2. Synthesis and evaluation of the new INH derivatives

We have previously studied the short (INH-C_2) and long (INH-C_{10}) chain acylated INH derivatives, which will be used in this work for comparative purposes. Several new INH derivatives from the two new series were synthesized in order to experimentally evaluate the computational results, namely a set of isonicotinoyl hydrazones derived from aliphatic aldehydes (hydrazone series), and another set corresponding to their reduced counterparts, the *N′*-alkyl hydrazides (alkyl hydrazide series).

The synthesis of the isonicotinoyl hydrazones was accomplished by a straightforward condensation of INH with commercially available aldehydes in ethanolic solution, under mild conditions. Reaction mixtures were maintained at room temperature for 24 h, leading to the corresponding Schiff bases in yields ranging from 64.8% to 92.1%, after purification by recrystallization. These reactions were easy to accomplish unlike the formation of other imines due to the stabilizing isonicotinoyl moiety which reduces the electrophilic character of the imine carbon, preventing the back-reaction. All compounds were characterized using IR, ^{1}H, ^{13}C NMR, COSY, HMQC, HMBC, NOESY, and HR-MS. The details of spectral data are given in the experimental section and spectra are provided in Figs. S1–S18 of Supplementary material.

In the NMR ^{1}H spectra (DMSO-d_6) of hydrazones (**2a–2e**), two sets of all protons were observed in a 1:0.1 ratio suggesting the presence of two species in solution. GC-MS and HPLC analyses of compounds established that, in all cases, only one isomer was present. We have previously reported that isonicotinoyl hydrazones derived from aromatic aldehydes had (*E*) configuration around the C═N double bond and, in solution, existed mainly as the synperiplanar CO—NH conformation [32]. For the Schiff bases reported herein, the assignment of the C═N configuration was hampered by the overlapping of the pyridine H-3 proton signal with that of the imine, as both have space correlations with the NH proton. The chemical shifts often change with temperature since this property induces variations in the compound conformational space. Therefore, variable-temperature NMR can facilitate the resolution of peaks from different conformers when they are significantly overlapped. For compound **2c**, NMR experiments were recorded at 25, 40, 50, and 60 °C, and we found that the separation of the two signals was complete at 50 °C. We also performed a NOESY experiment at 50 °C and the expected more stable (*E*) configuration was confirmed by the strong cross-peak between the azomethine and the NH signals, only possible in this configuration.

From the approaches reported in the literature to prepare hydrazides (**3a–3e**), the reduction of the corresponding Schiff bases is the most direct and versatile one, since it is accomplished in one step and takes advantage of the diversity allowed by several available aldehydes and ketones, which are useful to synthesize the hydrazones. Reduction of *N′*-acyl hydrazones may be achieved using sodium borohydride alone [33] or in combination with Amberlyst-15 (H^+) [34], sodium cyanoborohydride [35], or magnesium in methanol (MeOH) [36], among other reducing agents. All the mentioned methods were assayed, and we observed that the use of two equivalents of sodium cyanoborohydride, in refluxing methanol at pH 3, was the most suitable and selective procedure for the reduction of acyl hydrazones **2c–2e** although affording poor yields. Despite the rigorous control of the medium's pH, we could not circumvent over-reduction, which led to the *N′*,*N′*-dialkylated hydrazides as side products, probably through a mechanism analogous to the one observed for aldoximes [37].

In short, we have synthesized the complete hydrazone series (**2a–2e**) and several reduced derivatives from the alkyl hydrazide series (**3c–3e**) which were duly purified and characterized (see experimental). Stability assays carried out by UV–Vis, show that hydrazides are soluble and reasonably stable in 5% DMSO/water (> 90% remains after 24 h), whereas hydrazones decompose significantly within hours in the same conditions (e.g., **2d** degrades ~ 30% after 1.5 h). Hydrazones are known to hydrolyze, and this process can be accelerated by higher temperature or lower pH values [38]. To confirm this hypothesis for our hydrazones, we carried out several stability UPLC-MS/MS experiments in water for compound **2c**. In this case, the imine group hydrolyzed (~ 40% after 5 min; ~ 60% after 20 h) and we recovered back the starting material, i.e., INH.

KatG-induced kinetics of formazan formation using the nitroblue tetrazolium (NBT) assay, cytotoxicity towards HepG2 cells, MIC values against *Mtb*, as well as the therapeutic index (TI) taken as the ratio IC_{50}/MIC, are shown for many of these compounds in Table 2 (IC_{50} stands for the inhibitory concentration for 50% of the population).

3.3. The alkyl hydrazide series (INH-aC_n)

Our computational studies indicate that the INH hydrazide derivatives have a very high propensity to spontaneously form the IN* radical. This was confirmed by the kinetics experiments using the NBT assay where these compounds showed rates of formazan formation 2–3× or 8–16× higher than INH for the KatG-catalyzed or uncatalyzed reaction, respectively (Table 2). Interestingly, in this series, the presence of KatG does not have an impact on the rate of radical formation, probably because the hydrazide uncatalyzed reaction is already significantly faster than the fastest KatG accelerated process observed (INH). Having compounds with such high reactivity can be advantageous, but it is not without caveats. A question remains regarding how stable/effective these compounds will be in the cellular environment: will the spontaneously formed radicals reach the desired target (NADH) to generate the IN-NAD adduct, or will they react with unspecified targets *en route*? Furthermore, if the uncatalyzed reaction was dominant, we would lose all specificity that is conferred by the protein activation step. Altogether, these limitations can make the alkyl hydrazides less effective and/or more cytotoxic. Our results do show that the *N′*-alkylated INH derivatives are indeed more cytotoxic than INH (Table 2). INH, a compound known for its very low cytotoxicity (> 200 μM), contrasts with other approved antitubercular agents such as bedaquiline which has an IC_{50} of 17.4 μM [39]. Thus, a comparison of the IC_{50} values of the alkyl hydrazide derivatives with those of the aforementioned reference compounds indicates that the hydrazides may still be viable drugs. Here, their utility would depend on the trade-off (ratio) between cytotoxicity and MIC, usually quantified by the therapeutic index (TI) which is used

Table 2
Rates of formazan formation (nM/s) by INH derivatives evaluated from the NBT assay in the presence and absence of KatG, the ratio between both rates, IC_{50} values (μM) against HepG2 cells, and MIC values (μM) against the wild-type *Mtb* (H37Rv) and against the H37RvINH (Δ*katG*), a strain with full deletion of the *katG* gene. Also shown is the therapeutic index, TI.

Cpds	NBT assay with KatG[a] (nM/s)	NBT assay w/out KatG[a] (nM/s)	KatG factor	Cyto-toxicity IC_{50} (μM)[b]	*Mtb* H37Rv MIC (μM)	TI IC_{50}/MIC	*Mtb* H37RvΔ*katG* MIC (μM)
INH	6.8 ± 0.8	1.6 ± 0.5	4.3	> 200	0.3 [32]	> 667	933.4 [41]
INH-C_2	2.8 ± 2.0	0.8 ± 0.8	3.5	–	44.7 [32]	–	> 55.8 [32]
INH-C_{10}	0.4 ± 0.2	0.6 ± 0.6	–	> 25	0.5	> 50	> 34.3 [32]
INH-aC_6	22.3 ± 5.6	21.2 ± 18.0	1.1	39.8	4	10	> 128
INH-aC_8	15.2 ± 4.5	13.0 ± 9.2	1.2	23.2	–	–	–
INH-aC_{10}	20.6 ± 2.4	26.0 ± 17.0	0.8	48.0	2	24	128
INH-iC_4	2.1 ± 0.2	0.5 ± 0.2	4.2	> 200	–	–	–
INH-iC_6	–	–	–	> 200	0.3	> 667	> 128
INH-iC_8	2.5 ± 1.0	0.6 ± 0.6	4.2	> 100	–	–	–
INH-iC_{10}	2.2 ± 0.4	0.5 ± 0.5	4.4	> 25	0.3	> 667	128

[a] Values are average rates (nM/s) of two independent experiments with the range of the data representing the error.
[b] Chlorpromazine was used as positive control (IC_{50} = 13.9 μM).

to estimate the therapeutic window of a drug and to identify drug candidates for further studies [40].

The measured MIC values against H37Rv for INH-aC_6 and INH-aC_{10} are 4 and 2 μM, respectively, which are approximately an order of magnitude higher than that determined for INH (Table 2). This lower performance in stopping the *Mtb* growth could suggest that (1) the spontaneously formed radical is only partially reaching the NADH target, or (2) none reaches the target, and the reaction is fully catalyzed by KatG. The latter hypothesis is corroborated by the MIC values observed for the Δ*katG* mutant strain (⩾ 128 μM) (Table 2), which shows that KatG is pivotal in the activation of these compounds. Despite the weak overall performance, these two compounds show an uncommonly low minimum bactericidal concentration (MBC) against H37Rv (MBC = 64 and > 128 μM, respectively), suggesting a different mechanism of action that kills the mycobacteria instead of just preventing their growth, like in the case of INH (MBC = indeterminate) which is essentially bacteriostatic.

3.4. The hydrazone series (INH-iC_n)

The INH hydrazone derivatives showed *in silico* estimated reactivities similar to the reference compound, INH. In our kinetics experiments, the rates of formazan formation in the hydrazone series are about 3× slower than in INH, both in the presence and absence of KatG (Table 2). The rates of radical formation are slower than when using INH, which allows for a clear KatG-induced acceleration (~4×) for all hydrazone compounds as also seen with INH. Despite the lower reactivities, compounds from this series can still benefit from improved membrane permeabilities (Table 1) due to the presence of the lipophilic tails which improve the cell membrane crossing process, a phenomenon already observed for INH-C_{10} [7]. Their cytotoxicity values are also within the IC_{50} range observed for two compounds currently used in TB treatment, namely INH and bedaquiline, which make them relatively non-hepatotoxic.

The MIC values for the two tested hydrazone compounds (INH-iC_6 and INH-iC_{10}) are similar to that of INH for the wt strain (along with high values for the Δ*katG* strain), which raise several scenarios: either (1) there is an unlikely perfect trade-off between the lower reactivities and the improved membrane permeabilities due to their higher lipophilicity ($\log P_{O/W}$ = 1.54 ± 0.08 and 2.9 ± 0.2, respectively vs. −0.85 ± 0.01 for INH [42], where $P_{O/W}$ stands for the octanol-water partition coefficient); or (2) the hydrazone hydrolysis (recovering back INH) is occurring and is prevalent in a way that we are just measuring the effect of INH alone. The latter scenario seems more plausible as mentioned for compound **2d** by UPLC-MS/MS where over 60% hydrolysis takes place after 20 h. This indicates that the hydrazone hydrolysis occurs in the experimental conditions of MIC evaluation (several days) but not in the kinetics experiments (only a few minutes), where we observed a lower reaction rate than with INH. Furthermore, this hydrolysis step must be significantly faster than the KatG-catalyzed activation, since otherwise, it would have had a detrimental effect on the observed MIC values. The indeterminate MBC behavior for these two hydrazones, which is the same as for INH, also supports the scenario of their complete hydrolysis within the duration of these experiments. Nevertheless, hydrazone hydrolysis could still be used as a strategy to release INH inside cells [43]. In this hypothetical drug-delivery system, the aliphatic tail increases the lipophilicity of this prodrug, hence increasing its bioavailability inside the target cells, while a slow hydrolysis step would revert the compound to its active form. In principle, such a system would lead to lower MIC concentrations than INH, due to the increased cell trafficking. However, since we obtained similar MIC values, the data suggests that hydrolysis is too fast, and we end up measuring the INH inherent activity in cells. The hydrazone hydrolysis, which was assessed by HPLC to be less than 24 h, still allowed the measurement of the hydrazone kinetics (within minutes), but fully compromised the results obtained from the MIC experiments, which took several days to complete.

4. Conclusions

We have devised two new series of INH derivatives that showed promising *in silico* properties. Both shared an aliphatic carbon chain with similar sizes as the acyl hydrazide series (INH-C_n), which we had previously characterized using INH-C_2 and INH-C_{10} [7]. The rationale was the introduction of a long tail to improve the compound's lipophilic character and, consequently, increase its membrane permeability, which we identified as the key factor behind the good performance of INH-C_{10}. Our computational data indicated that substituting the *N'* acyl chains by the corresponding alkyl (hydrazides; INH-aC_n) or imine (hydrazones; INH-iC_n) moieties leads to an activation of the C—N bond, which is required to break in order to produce the isonicotinoyl radical. To evaluate these predictions, we synthesized various compounds from both series and performed kinetics, cytotoxicity, and MIC experiments.

The alkyl hydrazides showed impressively low energies in the QM calculations, suggesting a high reactivity towards the spontaneous radical formation. These results were confirmed in the stability and the NBT kinetic assays, where the compounds are decomposing, probably into the radical form, at a rate higher than the KatG-catalyzed reaction. However, the inferior performance in the MIC experiments, compared with INH, suggests that the higher number of radicals formed are not efficiently reaching NADH, which is their desired target inside the cells. On the other hand, compounds from the hydrazone series seem to be only slightly less reactive than INH. However, their possibly high hydrolysis rate may compromise their use in clinical settings, as suggested by the obtained MIC values, which can be attributed solely to INH, i.e.,

to the hydrolysis product.

In conclusion, our data shows that the two new series of INH derivatives are very reactive, in excellent agreement with our computational predictions. The alkyl hydrazides are probably too reactive, which appears to hinder their performance. This means that we could significantly benefit from less activated alkyl groups that would better balance the rate of IN* formation with a higher bioavailability in the target cells. The high rate of hydrolysis of the hydrazone compounds is also masking this series results, especially the MIC measurements that require several days to complete. Nevertheless, the systematic nature of this work allowed us to pinpoint the key factors behind the chemical nature of the aliphatic groups used to increase INH lipophilicity and simultaneously to recognize the need for a compromise in terms of enhanced reactivity. This knowledge will be pivotal to devise even better INH derivatives aimed at improving MIC performance and circumvent *Mtb* resistance to INH.

5. Experimental section

5.1. Chemistry

All organic solvents and reagents used throughout the procedures were purchased from commercial suppliers and used without additional purification. The course of the reactions was monitored by thin-layer chromatography performed on silica gel 60 F254 aluminum sheets (Ref. Merck 1.05554) and visualized with UV light at 254 nm. Flash column chromatography was performed on silica gel 60, 0.04–0.063 mm, 230–400 mesh (Ref. Merck 1.09385). ^{1}H NMR (400.1 MHz) and ^{13}C NMR spectra (100.6 MHz) were recorded on a Bruker® Avance™ 400 spectrometer, using DMSO-d_6 as solvent. Chemical shifts were expressed as δ (ppm) values and referenced to the residual solvent signal (δH = 2.50, δC = 39.51), coupling constants (J values) were reported in frequency units (Hz) and the following designations were used: s (singlet), d (doublet), t (triplet), q (quartet), m (multiplet). ^{1}H and ^{13}C assignments were made by 2D (COSY, HMQC, and HMBC) NMR experiments. The spectra treatment was performed using Bruker's TopSpin™ 3.1 software. HR-ESI-MS analyses were obtained on a hybrid quadrupole time-of-flight (QTOF) Bruker Impact II mass spectrometer at the IST node of the Portuguese Mass Spectrometry Network. IR spectra were recorded with 256 scans using Thermo Scientific™ Nicolet 6700 FT-IR spectrometer, equipped with a beam splitter and only the diagnostic bands were reported in cm^{-1}. Sample pellets were prepared in an approximate concentration of 1 mg/100 mg KBr.

The purity of all compounds (> 98%) was assessed by GC-MS analysis using Shimadzu® GCMS-QP2010 Plus, coupled with an autosampler AOC-20s, an automatic injector AOC-20i and a Teknokroma® Sapiens-5MS capillary column (30 m × 0.25 mm × 0.25 μm) packed with (95%) dimethyl (5%) diphenylpolysiloxane, and operating with an electron ionization (EI) source, using nitrogen as carrier gas at flow 1 mL/min, at a pressure of 63 bar. Samples were prepared either in dichloromethane or methanol, in an approximate concentration of 1 mg/mL, with one or more blanks of solvent being injected at the beginning of the analysis and between sample runs. Direct injection volume was 1 μL, at 280 °C; the GC oven was programmed at 100 °C (2 min), with a multi-step gradient temperature increase as follows: heated to 200 °C at 10 °C/min rate, then held at this temperature for 2 min, further heated to 300 °C at 10 °C/min rate and held at final temperature for 15 min; the mass spectrometer operated at 250 °C.

5.2. General procedure for the synthesis of isonicotinoyl hydrazones

The compounds were synthesized according to optimized protocols previously reported [32]. Briefly, 1 equivalent aldehyde was added drop-by-drop to a solution of isoniazid heat-dissolved in absolute ethanol, and the mixture was kept under agitation at room temperature for 24 h. Butanal, hexanal, octanal and decanal were the chosen aldehydes. The solvent was then evaporated under reduced pressure, affording the Schiff bases as crude white solids, and further recrystallized with ethyl acetate or acetone: MeOH 2:1 v/v to give crystalline white solids.

5.2.1. N′-(E)-ethylideneisonicotinohydrazide 2a

White crystals (recrystallization from dichloromethane/hexane) (η = 85%); IR (KBr), ν (cm^{-1}): 3232 (N—H amide), 3066 (arom. C—H), 2980–2918 (aliph. C—H), 1653 (C═O amide), 1622 (C═N imine); ^{1}H NMR (400 MHz, DMSO-d_6), δ (ppm): 11.68 (s, ^{1}H, NHC═O), 8.75 (d, 2H, J = 4.7 Hz, H-2, H-6), 7.75 (m, 3H, H-3, H-5, H-1′), 1.94 (d, 3H, J = 5.2 Hz, H-2′); ^{13}C NMR (100.6 MHz, DMSO-d_6): δ (ppm) = 161.25 (C═O), 150.32 (C-1′), 150.08 (C-2, C-6), 140.69 (C-4), 121.55 (C-3, C-5), 18.50 (C-2′). HR-ESI-MS: *m/z* 164.0822 [M + H]$^{+}$ (calcd. for $C_8H_9N_3O$ + H, 164.0818).

5.2.2. N′-(E)-butylideneisonicotinohydrazide 2b

White crystals (recrystallization from ethyl acetate) (η = 64.8%); IR (KBr), ν (cm^{-1}): 3199 (N—H amide), 3069 (arom. C—H), 2932–2870 (aliph. C—H), 1670 (C═O amide), 1633 (C═N imine); ^{1}H NMR (400 MHz, DMSO-d_6), δ (ppm): 11.65 (s, ^{1}H, NHC═O), 8.75 (d, 2H, J = 4.7 Hz, H-2, H-6), 7.75 (m, 3H, H-3, H-5, H-1′), 2.26 (m, 2H, H-2′), 1.53 (sext, 2H, J = 7.3Hz, H-3′), 0.93 (t, 3H, J = 7.3 Hz, H-4′); ^{13}C NMR (100.6 MHz, DMSO-d_6): δ (ppm) = 161.20 (C═O), 153.66 (C-1′), 150.27 (C-2, C-6), 140.67 (C-4), 121.49 (C-3, C-5), 33.97 (C-2′), 19.37 (C-3′), 13.65 (C-4′). HR-ESI-MS: *m/z* 192.1135 [M + H]$^{+}$ (calcd. for $C_{10}H_{13}N_3O$ + H, 192.1131).

5.2.3. N′-(E)-hexylideneisonicotinohydrazide 2c

Amorphous white powder (η = 81%); IR (KBr), ν (cm^{-1}) = 3230 (N—H amide), 3069 (arom. C—H), 2951–2868 (aliph. C—H), 1646 (C═O amide), 1625 (C═N imine); ^{1}H NMR (500 MHz, DMSO-d_6), δ (ppm): 11.65 (s, ^{1}H, NHC═O), 8.75 (d,d, 2H, J = 4.5; 1.5 Hz, H-2, H-6), 7.78 (t, ^{1}H, J = 5; H-1′), 7.75 (d, 2H, J = 4.3; H-3, H-5), 2.27 (dt, 2H, J = 7.3; 5.7 Hz, H-2′), 1.50 (quint, J = 7.3; Hz H-3′), 1.31 (m, 4H, H-4′, H-5′), 0.88 (t, 3H, H-6′); ^{13}C NMR (100.6 MHz, DMSO-d_6), δ (ppm): 161.24 (C═O), 153.84 (C-1′), 150.28 (C-2, C-6), 140.67 (C-4), 121.51 (C-3, C-5), 32.00 (C-2′), 30.90 (C-4′), 25.65 (C-3′), 21.94 (C-5′), 13.92 (C-6′). HR-ESI-MS: *m/z* 220.1447 [M + H]$^{+}$ (calcd. for $C_{12}H_{17}N_3O$ + H, 220.1444).

5.2.4. N′-(E)-octylideneisonicotinohydrazide 2d

White crystals (recrystallization from ethyl acetate) (η = 73.2%); IR (KBr), ν (cm^{-1}): 3204 (N—H amide), 3068 (arom. C—H), 2922–2854 (aliph. C—H), 1655 (C═O amide), 1624 (C═N imine); ^{1}H NMR (400 MHz, DMSO-d_6), δ (ppm): 11.64 (s, ^{1}H, NHC═O), 8.74 (d, 2H, J = 4.6 Hz, H-2, H-6), 7.74 (m, 3H, H-3, H-5, H-1′), 2.26 (m, 2H, H-2′), 1.49 (m, 2H, H-3′), 1.27 (m, 8H, H-4′ to H-7′), 0.86 (t, 3H, H-8′); ^{13}C NMR (100.6 MHz, DMSO-d_6): δ (ppm) = 161.23 (C═O), 153.85 (C-1′), 150.27 (C-2, C-6), 140.66 (C-4), 121.50 (C-3, C-5), 32.02 (C-2′), 31.22 (C-6′), 28.64, 28.51 (C-4′, C-5′), 25.97 (C-3′), 22.10 (C-7′), 13.98 (C-8′). HR-ESI-MS: *m/z* 248.1762 [M + H]$^{+}$ (calcd. for $C_{14}H_{21}N_3O$ + H, 248.1754).

5.2.5. N′-(E)-decylideneisonicotinohydrazide 2e

White crystals (recrystallization from ethyl acetate) (η = 92.1%); IR (KBr), ν (cm^{-1}): 3254 (N—H amide), 3075 (arom. C—H), 2925–2849 (aliph. C—H), 1655 (C═O amide), 1625 (C═N imine); ^{1}H NMR (400 MHz, DMSO-d_6), δ (ppm): 11.64 (s, ^{1}H, NHC═O), 8.75 (d, 2H, J = 4.8 Hz, H-2, H-6), 7.75 (m, 3H, H-3, H-5, H-1′), 2.26 (q, 2H, J = 6.7 Hz H-2′), 1.49 (m, 2H, H-3′), 1.25 (m, 10H, H-4′ to H-9′), 0.85 (t, 3H, H-10′); ^{13}C NMR (100.6 MHz, DMSO-d_6): δ (ppm) = 161.23 (C═O), 153.85 (C-1′), 150.27 (C-2, C-6), 140.67 (C-4), 121.50 (C-3, C-5), 32.02 (C-2′), 31.22 (C-8′), 28.95, 28.85, 28.72, 28.68 (C-4′ to C-7′), 25.96 (C-3′), 22.13 (C-9′), 14.00 (C-10). HR-ESI-MS: *m/z* 276.2075 [M + H]$^{+}$ (calcd.

for $C_{16}H_{25}N_3O$ + H, 276.2070).

5.3. General procedure for the synthesis of isonicotinoyl hydrazides [35]

Given the QM and MD results, just the most promising members of the series were synthesized, i.e., compounds **3c–3e**, as follows: two equivalents of $NaBH_3CN$ were added portion-wise to a solution of the parent hydrazone in methanol. Methanolic HCl 5 M was then progressively added until reaching pH 3, evidenced by a strong color change to dark yellow. The mixture was kept under reflux and agitation for several hours until the reaction was complete. Methanol was then evaporated under reduced pressure, giving an orange-yellow oil, to which a work-up procedure [adapted from [37]] was applied as follows: after the dissolution of the residue in water, a few drops of NaOH 6 M were added to basify the solution to pH > 7, destroying the possible cyanoborate adducts; after addition of brine, the solution was extracted several times with dichloromethane, the combined organic extracts were dried with $MgSO_4$ and the solvent evaporated under reduced pressure, affording crude yellowish solids which were further purified by column chromatography. White powders were then obtained and washed with hexane to remove small amounts of impurities.

5.3.1. N′-hexylisonicotinohydrazide 3c

Amorphous white powder (column chromatography with Et_2O: MeOH 98.2) η = 27.4%; IR (KBr): ν (cm^{-1}) = 3333 (N—H amide), 3018 (arom. C—H), 3000–2850 (aliph. C—H), 1635 (C═O amide); ^{1}H NMR (400 MHz, DMSO-d_6): δ (ppm) = 13.99 (s, 1H, NHC═O), 8.71 (d, 2H, J = 4.4 Hz, H-2, H-6), 7.73 (d, 2H, J = 4.4 Hz, H-3, H-5), 5.29 (s, 1H, $NHCH_2$), 2.78 (m, 2H, H-1′), 1.44 (m, 2H, H-2′), 1.31 (m, 6H, H-3′, H-4′, H-5′), 0.86 (t, 3H, H-6′); ^{13}C NMR (100.6 MHz, DMSO-d_6): δ (ppm) = 163.49 (C═O), 150.26 (C-2, C-6), 140.24 (C-4), 121.09 (C-3, C-5), 51.01 (C-1′), 31.24 (C-4′), 27.58 (C-2′), 26.34 (C-3′), 22.13 (C-5′), 13.99 (C-6′). HR-ESI-MS: *m/z* 222.1602 $[M + H]^+$ (calcd. for $C_{12}H_{19}N_3O$ + H, 222.1601).

5.3.2. N′-octylisonicotinohydrazide 3d

Amorphous white powder (column chromatography with Et_2O: MeOH 98.2) η = 47.3%; IR (KBr): ν (cm^{-1}) = 3265 (N—H amide), 3018 (arom. C—H), 2925–2871 (aliph. C—H), 1636 (C═O amide); ^{1}H NMR (400 MHz, DMSO-d_6): δ (ppm) = 10.29 (s, 1H, NHC═O), 8.70 (d, 2H, J = 4.4 Hz, H-2, H-6), 7.72 (d, 2H, J = 4.4 Hz, H-3, H-5), 5.25 (s, 1H, $NHCH_2$), 2.78 (m, 2H, H-1′), 1.44 (m, 2H, H-2′), 1.27 (m, 10H, H-3′ to H-7′), 0.85 (t, 3H, H-8′); ^{13}C NMR (100.6 MHz, DMSO-d_6): δ (ppm) = 163.45 (C═O), 150.24 (C-2, C-6), 140.21 (C-4), 121.06 (C-3, C-5), 50.96 (C-1′), 31.28 (C-6′), 28.94, 28.70 (C-4′, C-5′), 27.58 (C-2′), 26.64 (C-3′), 22.12 (C-7′), 13.99 (C-8′). HR-ESI-MS: *m/z* 250.1921 $[M + H]^+$ (calcd. for $C_{14}H_{23}N_3O$ + H, 250.1914).

5.3.3. N′-decylisonicotinohydrazide 3e

Amorphous white powder (column chromatography with AcOEt: MeOH 45:1) η = 32.9%; IR (KBr): ν (cm^{-1}) = 3330 (N—H amine), 3272 (N—H amide), 3028 (arom. C—H), 2917–2846 (aliph. C—H), 1640 (C═O amide); ^{1}H NMR (400 MHz, DMSO-d_6): δ (ppm) = 10.30 (s, 1H, NHC═O), 8.70 (d, 2H, J = 4.4 Hz, H-2, H-6), 7.72 (d, 2H, J = 4.4 Hz, H-3, H-5), 5.25 (s, 1H, $NHCH_2$), 2.77 (m, 2H, H-1′), 1.44 (m, 2H, H-2′), 1.23 (m, 14H, H-3′ to H-9′), 0.84 (t, 3H, J = 6.0 Hz, H-10′) ^{13}C NMR (100.6 MHz, DMSO-d_6): δ (ppm) = 163.43 (C═O), 150.22 (C-2, C-6), 140.19 (C-4), 121.04 (C-3, C-5), 50.96 (C-1′), 31.30 (C-8′), 29.03, 28.99, 28.96, 28.73 (C-4′ to C-7′), 27.57 (C-2′), 26.63 (C-3′), 22.11 (C-9′), 13.97 (C-10′). HR-ESI-MS: *m/z* 278.2235 $[M + H]^+$ (calcd. for $C_{16}H_{27}N_3O$ + H, 278.2227).

5.4. Stability evaluation by ultraperformance liquid chromatography-tandem mass spectrometry (UPLC-MS/MS)

Water stability of compound **2c** was accessed using an Elute ultra-high performance liquid chromatography system (Bruker, Bremen, Germany), equipped with a thermostatted autosampler, and interfaced with an ultra-high resolution quadrupole time-of-flight Impact II QTOF (Bruker, Bremen, Germany). Separations were performed on an intensity Solo 2 C18 RP column (100 × 2.1 mm, 2 μm; Bruker, Bremen, Germany) using a gradient of 0.1% (v/v) aqueous solution of formic acid (eluent A) and 0.1% (v/v) solution of formic acid in acetonitrile (eluent B), as follows: 0 min - 95% A; 1.5 min – 95% A; 13.5 min – 25% A; 18.5 min – 0% A; 21.5 min – 0% A; 23.5 min – 95% A; 30 min – 95% A. The column was then washed with 100% of eluent B for 5 min and reconditioned to initial conditions. The injection volume was set at 5 μL, the column was thermostatted at 35 °C and the flow rate was set at 0.250 mL/min. Spectral data were recorded in the *m/z* 50–1500 range. Electro-spray ionization in positive mode (4000 V capillary voltage, 6.0 mL drying gas flow at 200 °C, 10.0 eV collision cell energy) was used and MS/MS monitoring was chosen for detection. The internal standard solution was prepared, mixing 250 mL H_2O, 250 mL isopropyl alcohol (i-PrOH), 750 μL acetic acid, 250 μL formic acid and 0.5 mL 1 M NaOH solution. Data acquisition was carried out using the software Compass Data Analysis v.4.4 from Bruker. A solution of this compound (**2c**) at a concentration of 2.28×10^{-4} M was prepared by ultrasound-assisted dissolution at room temperature of 0.5 mg in 10 mL of MilliQ water. 5 μL of the sample solution was injected after 5 min of the beginning of dissolution. UPLC-MS chromatograms were acquired at 60, 120, 240 and 1200 min after the first injection.

5.5. In vitro kinetic assays

The KatG-dependent activation of isoniazid, as well as its hydrazide and hydrazone derivatives, was evaluated by monitoring radical formation. The radical formation was determined by monitoring the conversion of nitroblue tetrazolium (NBT) to its corresponding formazan at 560 nm (ϵ = 18,500 M^{-1} cm^{-1}) for 600 s in a solution with 1.25 μM KatG, 0.2 mM NBT, 0.2 μM $MnCl_2$, and 1.0 mM isoniazid or isoniazid derivative. All assays were carried out in 50% DMSO and 50 mM Tris-HCl, pH 8.0 at room temperature, and collected on a Shimadzu UV-Vis spectrophotometer. Results include two repeated experiments each with triplicate measurements. $MnCl_2$ and KatG-negative controls were included for each compound tested. Initial rates of NBT conversion to formazan were determined within the 35–40–100 s time window. The first 35–40 s of the raw traces contain features that are consistent with mixing artifacts and are therefore not included in the fitting and are represented by thin dotted lines (Fig. 3). The stimulatory effect of KatG was determined for NBT formazan formation by dividing the rates obtained with KatG by those obtained without.

5.6. Cytotoxicity towards HepG2 Cells

The *in vitro* toxicity of the studied compounds was evaluated using HepG2 cells, a human liver cancer cell line. HepG2 cells were plated on 384-well tissue culture-treated polystyrene plates at 2000 cells in 25 μL of HepG2 maintenance medium per well. After overnight incubation at 37 °C, the cells were dosed with test compounds and controls solubilized in dimethyl sulfoxide (DMSO) at a range of concentrations (dependent on the compound) and incubated for 72 h at 37 °C. The aqueous solubility of the compounds determined the range of concentrations tested. All compounds were solubilized in DMSO to 200-fold of the final top testing concentration. If compounds were soluble in DMSO (as for INH, INH-iC_4, INH-iC_6, INH-aC_6, INH-aC_8), aqueous solubility was tested using the medium at the top testing concentration (in these cases 200 μM) in a clear-bottom 96-well plate. For INH-C_{10}, INH-iC_8, INH-iC_{10}, and INH-aC_{10} the top testing concentration was 25, 100, 25, and 100 μM, respectively. Visual inspection was performed under a microscope for the identification of any precipitate. If precipitation was observed, DMSO volume in stock solution was doubled until acceptable aqueous solubility was found.

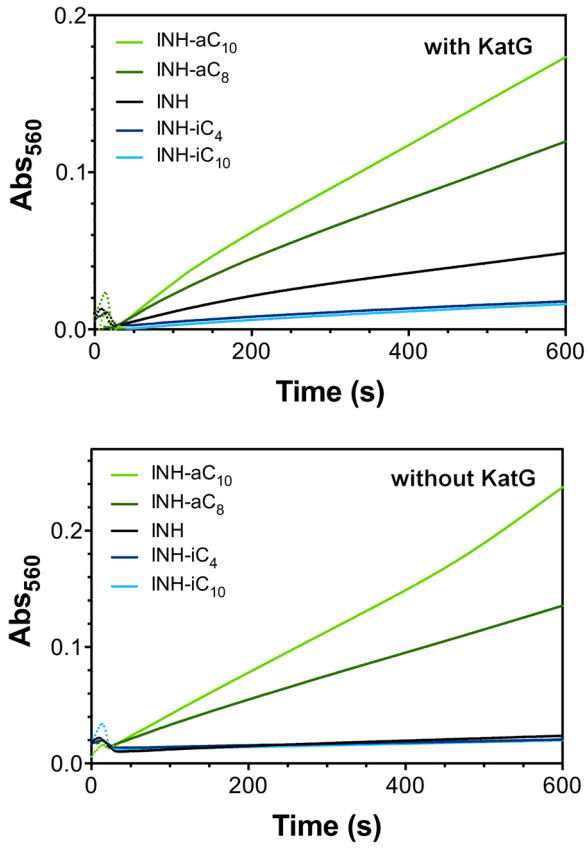

Fig. 3. Nitroblue tetrazolium (NBT) conversion to formazan by representative INH derivatives in the presence (top) and absence (bottom) of KatG. Isoniazid (INH), the hydrazide C8 (INH-aC$_8$; **3d**) and C10 (INH-aC$_{10}$; **3e**) derivatives, and the hydrazone C4 (INH-iC$_4$; **2b**) and C10 (INH-iC$_{10}$; **2e**) derivatives, each at 1.0 mM, were reacted in the presence of 0.2 μM $MnCl_2$ and 1.25 μM KatG. Each trace is the average of two experiments, each of which contained three replicates. Initial rates were determined 30–40 s after initiation of reactions in order to minimize interference from initial mixing phenomena. All reactions were carried out in 50 mM Tris-HCl and 50% DMSO, pH 8 at room temperature.

Cell viability was measured using the Promega CellTiter 96 Non-Radioactive Cell Proliferation Assay (MTT [44]) kit by adding the dye solution to each well and incubating for 3 h at 37 °C. After incubation, the solubilization solution/stop mix was added to each well. Plates were incubated at 37 °C for 1 h, mixed on a plate shaker for 10 min, and then absorbance read at 570 nm. Three independent replicates were performed for each compound concentration.

The concentration corresponding to 50% inhibition of cell viability, IC_{50}, was calculated with GraphPad Prism using a sigmoidal dose-response (variable slope) algorithm (see Fig. S19 of Supplementary material). Chlorpromazine, a well-known potent antipsychotic drug, was used as the positive control (IC_{50} = 13.9 μM).

5.7. Lipophilicity evaluation in terms of log $P_{o/w}$

Lipophilicity was assessed as the octanol-water partition coefficient (log $P_{o/w}$) determined by the shake-flask method, using the same procedure as previously described [32,42]. For both INH-iC$_6$ and INH-iC$_{10}$, samples were dissolved in water-saturated octanol at pH 6.4 (KH_2PO_4/NaOH buffer) to ensure negligible ionization. The partition to octanol-saturated aqueous buffer was measured, at room temperature, using a volume ratio, $r_{o/w}$, of 5/30 and 10/30, after 10 min sonication and 3 h partition on an in-house built mechanical tumbler. Equilibrium concentration was obtained by UV–Vis spectrophotometry between 200 and 500 nm after phase separation (5 min centrifugation).

5.8. Microbiology studies

Primary cultures: *Mtb* H37Rv was inoculated in mycobacteria growth indicator tubes (MGIT; Becton Dickinson, Sparks, MD, USA) supplemented with 10% OADC. The OADC supplement (from Becton Dickinson) contains oleic acid, bovine albumin, dextrose, and catalase. Oleic acid and other long-chain fatty acids are essential for mycobacteria metabolism, while dextrose is an energy source. Catalase neutralizes toxic peroxides and albumin also protects the mycobacteria from several toxic agents. The final tubes were incubated at 37 °C in the BACTEC MGIT 960 (MGIT 960; Becton Dickinson) system until they reached 100–200 growth units (GUs) and used directly for testing. Cultures with 200 > GU < 2000 were diluted to 100–200 GU with a sterile saline solution and used for testing. Growth of the cultures was monitored with the Epicenter V5.80A software equipped with the TB eXIST module (Becton Dickinson).

MIC and MBC determination: the MGITs were inoculated with 0.8 mL of OADC, 0.1 mL of the compound at the desired concentration and 0.5 mL of the suspension of the strain. The compounds were prepared at two-fold serial dilutions to obtain concentrations ranging from 0.03125 to 128 μM. For preparation of the drug-free proportional control, the primary culture was diluted 1:100 with a sterile saline solution and 0.5 mL inoculated in the tube. The drug-free absolute control was inoculated with 0.5 mL of the undiluted culture. The drug-containing tubes with > 100 GU when the proportional control reached 400 GU were resistant to the corresponding concentration. If the GU of the tube containing the drug was < 100 GU they were susceptible. The minimum bactericidal concentration (MBC) was determined with the MGIT 960 and defined as the concentration that prevents *Mtb* growth after 100 days of incubation at 37 °C [45].

CRediT authorship contribution statement

Catarina Frazão de Faria: Investigation, Writing – original draft. **Tânia Moreira:** Investigation. **Pedro Lopes:** Investigation, Methodology, Writing – original draft. **Henrique Costa:** Investigation. **Jessica R. Krewall:** Investigation, Methodology, Writing – original draft. **Callie M. Barton:** Investigation. **Susana Santos:** Data curation, Methodology, Supervision, Writing – original draft, Writing – review & editing. **Douglas Goodwin:** Data curation, Funding acquisition, Supervision, Writing – original draft, Writing – review & editing. **Diana Machado:** Investigation, Methodology, Writing – original draft. **Miguel Viveiros:** Data curation, Funding acquisition, Supervision, Writing – review & editing. **Miguel Machuqueiro:** Conceptualization, Data curation, Funding acquisition, Software, Supervision, Writing – original draft, Writing – review & editing. **Filomena Martins:** Conceptualization, Data curation, Funding acquisition, Project administration, Supervision, Writing – original draft, Writing – review & editing.

Conflict of interest statement

There are no conflicts of to declare.

Acknowledgments

We acknowledge Diogo Vila Viçosa for valuable discussions. We acknowledge financial support from Fundação para a Ciência e a Tecnologia, Portugal through projects PTDC/MED-QUI/29036/2017, PTDC/BIA-MIC-30692/2017, UIDB/00100/2020, UIDP/00100/2020, UIDB/04046/2020, UIDP/04046/2020, and UID/Multi/04413/2020, and Grants CEECIND/02300/2017 and DL57/CEECIND/0256/2017. Contributions from JRK, CMB, and DCG supported in part by a grant from the National Science Foundation, USA (MCB 1616059).

Appendix A. Supplementary material

Supplementary data associated with this article can be found in the online version at doi:10.1016/j.biopha.2021.112362.

References

[1] World Health Organization, Global Tuberculosis Report 2020. ⟨https://apps.who.int/iris/bitstream/handle/10665/336069/9789240013131-eng.pdf⟩. (Accessed 22 May 2021).

[2] Stop TB Partnership, Stop TB Partnership Media Brief, 2021. ⟨http://www.stoptb.org/webadmin/cms/docs/20210316_TB⟩ and COVID_One Year on_Media Brief_FINAL.pdf. (Accessed 22 May 2021).

[3] C. Vilchèze, W.R. Jacobs Jr., The isoniazid paradigm of killing, resistance, and persistence in mycobacterium tuberculosis, J. Mol. Biol. 431 (18) (2019) 3450–3461.

[4] A. Banerjee, E. Dubnau, A. Quemard, V. Balasubramanian, K.S. Um, T. Wilson, D. Collins, G. De Lisle, W.R. Jacobs, Inha, a gene encoding a target for isoniazid and ethionamide in mycobacterium tuberculosis, Science 263 (5144) (1994) 227–230.

[5] K.A. Abrahams, G.S. Besra, Synthesis and recycling of the mycobacterial cell envelope, Curr. Opin. Microbiol. 60 (2021) 58–65.

[6] C. Lange, K. Dheda, D. Chesov, A.M. Mandalakas, Z. Udwadia, C.R. Horsburgh Jr, Management of drug-resistant tuberculosis, Lancet 394 (10202) (2019) 953–966.

[7] D. Vila-Vicosa, B.L. Victor, J. Ramos, D. Machado, M. Viveiros, J. Switala, P. C. Loewen, R. Leitao, F. Martins, M. Machuqueiro, Insights on the mechanism of action of INH-C_{10} as an antitubercular prodrug, Mol. Pharm. 14 (12) (2017) 4597–4605.

[8] Y. Zhao, D.G. Truhlar, Exploring the limit of accuracy of the global hybrid meta density functional for main-group thermochemistry, kinetics, and noncovalent interactions, J. Chem. Theory Comput. 4 (11) (2008) 1849–1868.

[9] T.H. Dunning Jr., Gaussian basis sets for use in correlated molecular calculations. I. The atoms boron through neon and hydrogen, J. Chem. Phys. 90 (2) (1989) 1007–1023.

[10] R.A. Kendall, T.H. Dunning Jr., R.J. Harrison, Electron affinities of the first-row atoms revisited. Systematic basis sets and wave functions, J. Chem. Phys. 96 (9) (1992) 6796–6806.

[11] A.V. Marenich, C.J. Cramer, D.G. Truhlar, Universal solvation model based on solute electron density and on a continuum model of the solvent defined by the bulk dielectric constant and atomic surface tensions, J. Phys. Chem. B 113 (18) (2009) 6378–6396.

[12] V.H. Teixeira, D. Vila-Vicosa, A.M. Baptista, M. Machuqueiro, Protonation of dmpc in a bilayer environment using a linear response approximation, J. Chem. Theory Comput. 10 (5) (2014) 2176–2184.

[13] V.H. Teixeira, D. Vila-Viçosa, P.B. Reis, M. Machuqueiro, pK_a values of titrable amino acids at the water/membrane interface, J. Chem. Theory Comput. 12 (3) (2016) 930–934.

[14] M.J. Abraham, T. Murtola, R. Schulz, S. Páll, J.C. Smith, B. Hess, E. Lindahl, GROMACS: high performance molecular simulations through multi-level parallelism from laptops to supercomputers, SoftwareX (1–2) (2015) 19–25.

[15] W.R.P. Scott, P.H. Hünenberger, I.G. Tironi, A.E. Mark, S.R. Billeter, J. Fennen, A. E. Torda, T. Huber, P. Krüger, W.F. van Gunsteren, The GROMOS biomolecular simulation program package, J. Phys. Chem. A 103 (19) (1999) 3596–3607.

[16] N. Schmid, A.P. Eichenberger, A. Choutko, S. Riniker, M. Winger, A.E. Mark, W. F. van Gunsteren, Definition and testing of the GROMOS force-field versions 54A7 and 54B7, Eur. Biophys. J. 40 (7) (2011) 843.

[17] J. Hermans, H.J.C. Berendsen, W.F.V. Gunsteren, J.P.M. Postma, A consistent empirical potential for water-protein interactions, Biopolymers 23 (8) (1984) 1513–1518.

[18] K.B. Koziara, M. Stroet, A.K. Malde, A.E. Mark, Testing and validation of the automated topology builder (ATB) version 2.0: prediction of hydration free enthalpies, J. Comput. Aided Mol. Des. 28 (3) (2014) 221–233.

[19] H.A. Filipe, C. Sousa, J.T. Marques, D. Vila-Viçosa, A. de Granada-Flor, A.S. Viana, M.S.C. Santos, M. Machuqueiro, R.F. de Almeida, Differential targeting of membrane lipid domains by caffeic acid and its ester derivatives, Free Radic. Biol. Med. 115 (2018) 232–245.

[20] N.F. Oliveira, I.D. Pires, M. Machuqueiro, Improved GROMOS 54A7 charge sets for phosphorylated Tyr, Ser, and Thr to deal with pH-dependent binding phenomena, J. Chem. Theory Comput. 16 (10) (2020) 6368–6376.

[21] M. Stark, T.F. Silva, G. Levin, M. Machuqueiro, Y.G. Assaraf, The lysosomotropic activity of hydrophobic weak base drugs is mediated via their intercalation into the lysosomal membrane, Cells 9 (5) (2020) 1082.

[22] M. Parrinello, A. Rahman, Polymorphic transitions in single crystals: a new molecular dynamics method, J. Appl. Phys. 52 (12) (1981) 7182–7190.

[23] S. Nosé, M.L. Klein, Constant pressure molecular dynamics for molecular systems, Mol. Phys. 50 (5) (1983) 1055–1076.

[24] G. Bussi, D. Donadio, M. Parrinello, Canonical sampling through velocity rescaling, J. Chem. Phys. 126 (1) (2007), 014101.

[25] B. Hess, P-LINCS: a parallel linear constraint solver for molecular simulation, J. Chem. Theory Comput. 4 (1) (2008) 116–122.

[26] S. Miyamoto, P.A. Kollman, Settle: an analytical version of the SHAKE and RATTLE algorithm for rigid water models, J. Comput. Chem. 13 (8) (1992) 952–962.

[27] J.S. Hub, B.L. De Groot, D. Van Der Spoel, g_wham – a free weighted histogram analysis implementation including robust error and autocorrelation estimates, J. Chem. Theory Comput. 6 (12) (2010) 3713–3720.

[28] J.M. Diamond, Y. Katz, Interpretation of nonelectrolyte partition coefficients between dimyristoyl lecithin and water, J. Membr. Biol. 17 (1) (1974) 121–154.

[29] S.-J. Marrink, H.J. Berendsen, Simulation of water transport through a lipid membrane, J. Phys. Chem. 98 (15) (1994) 4155–4168.

[30] G. Hummer, Position-dependent diffusion coefficients and free energies from bayesian analysis of equilibrium and replica molecular dynamics simulations, New J. Phys. 7 (1) (2005) 34.

[31] C.J. Dickson, V. Hornak, R.A. Pearlstein, J.S. Duca, Structure-kinetic relationships of passive membrane permeation from multiscale modeling, J. Am. Chem. Soc. 139 (1) (2017) 442–452.

[32] F. Martins, S. Santos, C. Ventura, R. Elvas-Leitão, L. Santos, S. Vitorino, M. Reis, V. Miranda, H.F. Correia, J. Aires-de Sousa, et al., Design, synthesis and biological evaluation of novel isoniazid derivatives with potent antitubercular activity, Eur. J. Med. Chem. 81 (2014) 119–138.

[33] J.H. Billman, A.C. Diesing, Reduction of schiff bases with sodium borohydride, J. Org. Chem. 22 (9) (1957) 1068–1070.

[34] J.R. Caycho, F.G. Tellado, P. de Armas, J. Juan, M. Tellado, Sodium borohydride-amberlyst-15 (H.): an effective reductor for hindered and unreactive ketones in aprotic solvent, Tetrahedron Lett. 38 (2) (1997) 277–280.

[35] R. Maccari, R. Ottana, F. Monforte, M.G. Vigorita, In vitro antimycobacterial activities of 2′-monosubstituted isonicotinohydrazides and their cyanoborane adducts, Antimicrob. Agents Chemother. 46 (2) (2002) 294–299.

[36] J.M. Khurana, B. Kandpal, P. Sharma, M. Gupta, A novel method of reduction of c=n- group in hydrazones, phenylhydrazones, azines, and tosylhydrazones by Mg-methanol, Mon. Chem. 146 (1) (2015) 187–190.

[37] R.F. Borch, M.D. Bernstein, H.D. Durst, Cyanohydridoborate anion as a selective reducing agent, J. Am. Chem. Soc. 93 (12) (1971) 2897–2904.

[38] N.J. Lees-Gayed, M.A. Abou-Taleb, I.A. El-Bitash, M.F. Iskander, Studies on biologically active acylhydrazones. Part 1. Acid-base equilibria and acid hydrolysis of pyridoxal aroylhydrazones and related compounds, J. Chem. Soc. Perkin Trans. 2 (2) (1992) 213–217.

[39] A. Lupien, A. Vocat, C.S.-Y. Foo, E. Blattes, J.-Y. Gillon, V. Makarov, S.T. Cole, Optimized background regimen for treatment of active tuberculosis with the next-generation benzothiazinone macozinone (PBTZ169), Antimicrob. Agents Chemother. 62 (11) (2018) e00840–18.

[40] F.R. Pavan, P.I.d.S. Maia, S.R. Leite, V.M. Deflon, A.A. Batista, D.N. Sato, S. G. Franzblau, C.Q. Leite, Thiosemicarbazones, semicarbazones, dithiocarbazates and hydrazide/hydrazones: anti-mycobacterium tuberculosis activity and cytotoxicity, Eur. J. Med. Chem. 45 (5) (2010) 1898–1905.

[41] D. Machado, I. Couto, J. Perdigão, L. Rodrigues, I. Portugal, P. Baptista, B. Veigas, L. Amaral, M. Viveiros, Contribution of efflux to the emergence of isoniazid and multidrug resistance in mycobacterium tuberculosis, PLOS ONE 7 (4) (2012), e34538.

[42] C. Rafóls, E. Bosch, R. Ruiz, K.J. Box, M. Reis, C. Ventura, S. Santos, M.E. Araújo, F. Martins, Acidity and hydrophobicity of several new potential antitubercular drugs: isoniazid and benzimidazole derivatives, J. Chem. Eng. Data 57 (2) (2012) 330–338.

[43] D.K. Kölmel, E.T. Kool, Oximes and hydrazones in bioconjugation: mechanism and catalysis, Chem. Rev. 117 (15) (2017) 10358–10376.

[44] Riss T.L., Moravec R.A., Niles A.L., Duellman S., Benink H., Worzella T., Minor L., et al., Cell Viability Assays, Eli Lilly & Company and the National Center for Advancing Translational Sciences, 2016.

[45] P. Filippini, E. Iona, G. Piccaro, P. Peyron, O. Neyrolles, L. Fattorini, Activity of drug combinations against dormant mycobacterium tuberculosis, Antimicrob. Agents Chemother. 54 (6) (2010) 2712–2715.